Macromolecules

ARTICLE

pubs.acs.org/Macromolecules

Heterogeneity of the Segmental Dynamics in Lamellar Phases of Diblock Copolymers

Mohammed Zakaria Slimani,[†] Angel J. Moreno,[*,‡] and Juan Colmenero[†,‡,§]

[†]Donostia International Physics Center, Paseo Manuel de Lardizabal 4, E-20018 San Sebastián, Spain

[‡]Centro de Física de Materiales (CSIC, UPV-EHU) and Materials Physics Center MPC, Paseo Manuel de Lardizabal 5, E-20018 San Sebastián, Spain

[§]Departamento de Física de Materiales, Universidad del País Vasco (UPV-EHU), Apartado 1072, E-20080 San Sebastián, Spain

ABSTRACT: By means of computer simulations, we investigate the segmental dynamics in the lamellar phase of a simple bead−spring model of diblock copolymers. We characterize the dynamic heterogeneity in the mean-squared displacements and bond reorientations. This characterization is made as a function of both the position of the monomers along the chain and the distance to the nearest interface between consecutive domains. Both characterizations of the dynamic heterogeneity reveal moderate gradients of mobility in the investigated temperature range, which qualitatively probes relaxation time scales of up to hundreds of nanoseconds. Namely, the obtained distribution of relaxation times spreads over about 1 decade. However, the extrapolation of the former analysis to lower temperatures leads to an increasing spread over several time decades. The spread mostly arises from monomers located at the immediate neighborhood of the interface. Beyond such distances the structural relaxation approaches that of the homopolymer. Thus, the observed dynamic heterogeneity is esentially an interfacial effect. It does not originate from gradients of density over the domains. Indeed such gradients are absent, and the local density within the domains is identical to that of the corresponding homopolymers.

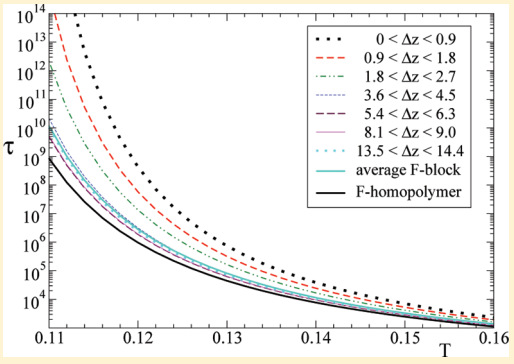

I. INTRODUCTION

Diblock copolymers of thermodynamically immiscible components can exhibit microphase separation in domains rich in one component and poor in the other. The domains can be arranged in ordered periodic structures, leading to phases with, e.g., lamellar, cylinder, spherical or gyroid morphologies.[1−6] The transition from the disordered to the ordered state and between the different ordered phases can be easily tuned by changing control parameters as the temperature, chain length, or monomer fraction of each component.

Several dynamic features in ordered phases of diblock copolymers have been investigated in cylinder,[7−11] gyroid,[8,12] spherical,[13−20] and mostly lamellar morphology.[7,12,21−43] In lamellae-forming systems the diffusivity exhibits a bifurcation, around the order−disorder transition, in two components parallel and perpendicular to the lamellar planes. This bifurcation is smooth, and the diffusivity shows no discontinuity. For the case of nonentangled chains, diffusion in the lamellar phase is strongly anisotropic, with a strong reduction of the perpendicular component.[22,32−34] On the other hand, for entangled chains differences between perpendicular and parallel diffusivities are strongly reduced.[23,24,27,35]

Concerning the local segmental dynamics, i.e., the α-structural relaxation associated with the glass transition,[44,45] a general observation is that the α-relaxation times in the lamellar phase are close to those of the corresponding homopolymer.[30,36,38,40,41,43] Usually, the former are slightly shifted to shorter or longer values than in the homopolymer if the segmental dynamics of the other block is respectively faster or slower, i.e., if the other block has a lower or higher glass transition temperature T_g. Despite the similar values of the α-time scales, the dynamic response in the lamellar phase exhibits a strong broadening in the low-frequency side (long times) in comparison with the corresponding homopolymer. This effect is particulary visible by means of broadband dielectric spectroscopy (BDS),[36,38,41,43] which reveals a progressive broadening by several frequency decades on decreasing temperature. This feature is usually rationalized in terms of dynamic heterogeneity. It is assumed that the segmental relaxation in the center of the lamellar domains is esentially the same as in the corresponding homopolymer. However, the former is strongly perturbed as the lamellar interface is approached, leading to gradients of mobility.[38] The density jump occurring at the interface induces such a strong perturbation that propagates into each phase. This proposed microscopic picture has connections with the scenario observed for dense polymer brushes,[46,47] polymer melts confined in slits,[48,49] and free-standing or supported polymer thin films,[50−53] where density jumps at the interface are even more abrupt than in lamellar phases of diblock

Received: February 27, 2011
Revised: July 15, 2011
Published: August 04, 2011

copolymers. More generally, it has connections with dynamic features of the structural relaxation in confined fluids.[54−56]

In this article we present a detailed characterization of the heterogeneity of the segmental dynamics in lamellar phases. We study this feature by means of molecular dynamics simulations of a generic bead−spring model of diblock copolymers. Aiming to mimic usual experimental systems,[21,25,30,37,38,41] the corresponding homopolymers exhibit very different intrinsic mobilities, i.e., different glass transition temperatures. The simulations are performed in the strongly segregated regime, with a well-defined lamellar morphology. We characterize the dynamic heterogeneity as a function of both the monomer location along the chain and the distance to the nearest interface between consecutive domains. Both characterizations of the dynamic heterogeneity reveal moderate gradients of mobility, of about one time decade, in the investigated temperature range, which qualitatively probes relaxation time scales of up to hundreds nanoseconds. However, the extrapolation of the results to lower temperatures leads to an increasing spread over several time decades. This spread originates mostly from monomers located at the immediate neighborhood of the interface. Beyond such distances the structural relaxation approaches that of the homopolymer. Thus, we conclude that the observed dynamic heterogeneity is esentially an interfacial effect. It does not originate from gradients of density over the domains. Indeed such gradients are absent, and the local density within the domains is identical to that of the corresponding homopolymers.

The article is organized as follows. In section II we describe the investigated model and give simulation details. In section III we characterize static and dynamic properties of the lamellar phase. In section IV we discuss and compare our simulations with experimental results in the literature. Conclusions are given in section V.

II. MODEL AND SIMULATION DETAILS

We simulate polymer melts of identical bead−spring chains of $N = 350$ monomers. The simulation box contains $N_{cha} = 136$ chains. The diblock systems have symmetric composition. Thus, each diblock chain consists of $N_F = N_S = 175$ monomers of respectively the species F ("fast") and S ("slow"). The interaction between any two given monomers of the species α and $\beta \in \{F,S\}$ is given by a shifted Lennard-Jones potential:

$$V_{\alpha\beta}(r) = 4\varepsilon_{\alpha\beta}\left[\left(\frac{\sigma_{\alpha\beta}}{r}\right)^{12} - \left(\frac{\sigma_{\alpha\beta}}{r}\right)^{6} + \frac{1}{4}\right] \quad (1)$$

for $r < r_c$ and $V_{\alpha\beta}(r) = 0$ for $r \geq r_c$. By using a value $r_c = 2^{1/6}\sigma_{\alpha\beta}$ for the cutoff distance, the potential is purely repulsive and has no local minima. Moreover, potential and forces are continuous at r_c. In addition to the Lennard-Jones potential, two connected monomers in a same chain interact through a finitely extensible nonlinear elastic potential (FENE):[57]

$$V_{\alpha\beta}^{FENE}(r) = -\varepsilon_{\alpha\beta}K_F{R_0}^2 \ln\left[1 - \left(\frac{r}{R_0\sigma_{\alpha\beta}}\right)^2\right] \quad (2)$$

with $K_F = 15$ and $R_0 = 1.5$. The sum of the potentials (1) and (2) yields an effective potential between connected monomers which shows a sharp minimum at $r = 0.96\sigma_{\alpha\beta}$ and guarantees chain uncrossability.[57] We use identical monomer masses $m_F = m_S = m = 1$ and interaction diameters $\sigma_{FF} = \sigma_{SS} = \sigma_{FS} = \sigma = 1$. In order to obtain different mobilities for the two species, we use different values for the energy scale of the self-interaction, $\varepsilon_{FF} = 0.35$ and $\varepsilon_{SS} = 1$, which leads to faster dynamics for the F-component (see below). For the cross-interaction we use $\varepsilon_{FS} = 9$. With this strong energetic penalty for the F−S interactions and the used long chains, the diblock system is expected to be in the strongly segregated regime at temperatures of interest.[34] In spite of the used symmetric composition $N_F = N_S = 175$, the different self-interactions $\varepsilon_{FF} = 0.35$ and $\varepsilon_{SS} = 1$ lead to a certain asymmetric character of the copolymer (unlike in e.g., ref 34, where the parameters for both self-interactions are identical). However, the system clearly remains inside the lamellar region of the phase diagram (see below).

In the following, temperature T, pressure P, monomer number density ρ, time t, and distance will be given respectively in units of ε_{SS}/k_B (with k_B the Boltzmann constant), $\varepsilon_{SS}\sigma^{-3}$, σ^{-3}, $\sigma(m/\varepsilon_{SS})^{1/2}$, and σ. Simulation units for distance and time can be qualitatively mapped to real units as $\sigma \sim 5-10$ Å and $\sigma(m/\varepsilon)^{1/2} \sim 1-10$ ps (see the discussion in, e.g., refs 48 and 57).

For the homopolymer systems we use a cubic simulation box with periodic boundary conditions. Computation time is reduced by using a linked-cell method[58] for calculation of interparticle distances within interaction ranges. We perform an initial run in the isothermal−isobaric (NPT) ensemble at external pressure $P_{ex} = 3.0$ by using the Nosé−Hoover algorithm.[58] A further equilibration run is performed at constant volume under periodic velocity scaling, according to the target temperature. Finally, a run is performed in the microcanonical ensemble for production of configurations,[59] from which we compute the static and dynamic observables presented below. Equations of motion are integrated in the Martyna's scheme[58,60] for the NPT runs and in the velocity-Verlet scheme[58] for the other runs. We use typical integration time steps of $2 \times 10^{-3} \leq \delta t \leq 4 \times 10^{-3}$, according to the investigated temperature. The latter covers the range $0.14 \leq T \leq 0.30$. The corresponding equilibrium densities for $P_{ex} = 3.0$ cover the range $1.06 \geq \rho \geq 0.98$ and $1.00 \geq \rho \geq 0.92$ for respectively the F- and S-homopolymer. These are typical melt densities for similar bead−spring models of polymer systems.[48,57]

A different equilibration procedure is needed in the case of the lamellar phase of the diblock system. Except for rather short chains at high temperature, the spontaneous formation in the melt state of well-ordered mesophases, by starting from a disordered configuration, is unfeasible within simulation time scales.[19,29,34,61] Thus, spontaneous evolution generally leads to a metastable microsegregated phase, which may exhibit the expected geometry of the segregated domains at short and even middle length scales, but lacks of large-scale order.[19,29] The usual strategy for obtaining ordered phases is actually to equilibrate the system by starting from a configuration with the expected geometry.[34,62−64] Thus, we have followed a procedure based on the method proposed by Schultz et al.[64] The simulation cell is orthoedric, of sides $L_x = L_y \neq L_z$, with z the coordinate perpendicular to the lamellar planes. We first set four equidistant F−S interfaces in the simulation cell. Then, starting from the parallel planes representing the interfaces, S- and F-blocks are constructed by chain grow-up. Thus, all the S-blocks linked to a same interface grow up over the same z-direction, and the respective F-blocks grow up over the opposite one. Blocks of the same species and linked to consecutive interfaces grow up over opposite directions, leading to a sequence of blocks SF-FS-SF-FS...

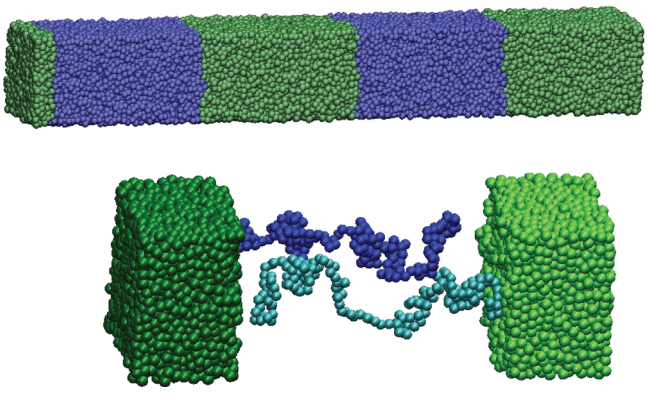

Figure 1. Top: typical snapshot of the lamellar phase. F- and S-monomers are represented respectively in blue and green. Bottom: typical conformations of two F-blocks (blue, center of the figure). The S-domains (green) to which they are linked are partially represented at the left and right sides of the figure. Light and dark F-blocks are respectively linked to light and dark S-domains.

along the z-direction (see Figure 1). A constraint is imposed in the grow-up procedure in order to avoid core overlap of new monomers with previously inserted ones. The same number of chains, $N_{cha}/4$, is constructed at each interfacial plane.

We select a volume $V = L_xL_yL_z$ for the initial simulation box in order to get an initial density $\rho = N_{cha}N/V \sim 0.5$. Then we start a run in the *NPT* ensemble as described above, at the same $P_{ex} = 3.0$. Since volume fluctuations are isotropic in this method (i.e, the three cell axes are rescaled by the same factor[58]), it is clear that the correct equilibrium lamellar spacing can only be achieved fortuitously. Thus, isotropic volume fluctuations will in general produce an unbalance between the components of the internal pressure, $\langle P_x\rangle = \langle P_y\rangle \neq \langle P_z\rangle$. In order to balance the three components, we periodically apply a box length search algorithm,[64] which maintains the instantaneous volume, but rescale the z-coordinate by a factor $1 - |\xi| \leq f \leq 1 + |\xi|$, and simultaneously the x,y-coordinates by a factor $f^{-1/2}$. We use $f > 1$ when $\langle P_{x,y}\rangle' < \langle P_z\rangle'$ and $f < 1$ when $\langle P_{x,y}\rangle' > \langle P_z\rangle'$. Here $\langle ...\rangle'$ denotes average over a certain interval prior to the next rescaling. We initially take $|\xi| \lesssim 0.01$ and progressively decrease its value as the pressure balance $\langle P_x\rangle = \langle P_y\rangle = \langle P_z\rangle = P_{ex}$ is approached. Once this is achieved we perform, as described above, a further equilibration run at constant volume under periodic velocity scaling, and a final production run in the microcanonical ensemble. We investigate the same temperature range $0.14 \leq T \leq 0.30$ as for the homopolymers. The obtained equilibrium densities of the lamellar domains are equal, within statistics, to those of the respective homopolymers (see section III).

Typical simulation times for both equilibration and production runs are of 30 million integration time steps. In absolute units the latter typically cover up to time scales of $t \sim 10^5$, which qualitativey correspond in real systems to several hundred nanoseconds (see above). Static profiles (see below) are averaged over configurations at typically 100 equispaced times. Dynamic observables are averaged over 20 equispaced time origins.

III. RESULTS

A. Static Properties. The top panel of Figure 1 shows a typical snapshot of the lamellar phase. The combination of isotropic box fluctuations with periodic anisotropic scaling (see section II)

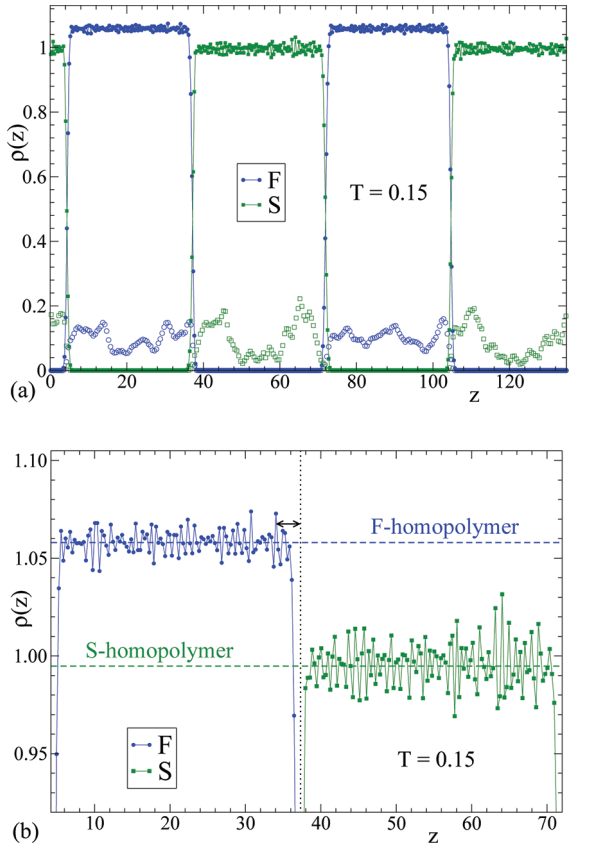

Figure 2. (a) Local density profiles $\rho(z)$ for the F- and S-monomers in the direction perpendicular to the lamellar planes, at $T = 0.15$. Filled symbols (higher data sets) correspond to data for all monomers of each species. Empty symbols (lower data sets) correspond to data for end monomers, namely for the 10% closest to the chain ends ($i < 18$ and $i > 333$). Note that accordingly, the statistical noise is enhanced by a factor 10 in comparison with data of all monomers. (b) For clarity, data of all monomers in (a) are shown only for two selected layers. Also included are the macroscopic densities ρ_{hom} of the F- and S-homopolymers (thick dashed lines) at the same T. The vertical dotted line indicates the interface position. The arrow extends from the interface to a distance $\Delta z = 3\sigma$.

produces structures with well-defined order. We obtain stable ordered lamellar structures at all the investigated temperatures. The bottom panel of Figure 1 shows two typical conformations of the F-blocks, extending over a same F-domain and linked to different S-domains. The blocks do not show Gaussian conformations but are strongly stretched. In spite of the associated entropic penalty, stretched conformations are favored by the strong reduction of energetically unfavorable contacts between distinct blocks. This is a well-known feature for strongly segregated lamellae.[21,25,62,65]

We characterize local density profiles of each species (F and S) along the direction perpendicular to the lamellar planes. For this we introduce the quantity $\rho(z) = n(z)/[L_xL_y\delta]$, with bin size $\delta = 0.1\sigma$ and $n(z)$ the number of monomers of the considered species which are located in the interval $(z - \delta/2, z + \delta/2)$. Figure 2 displays the local density profile at $T = 0.15$. Sharp boundaries are observed between the F- and S-domains, as expected for the strongly segregated regime. The domain size at $T = 0.15$ is about 33σ, which qualititatively corresponds to about 15−35 nm in real systems (see section II). As observed

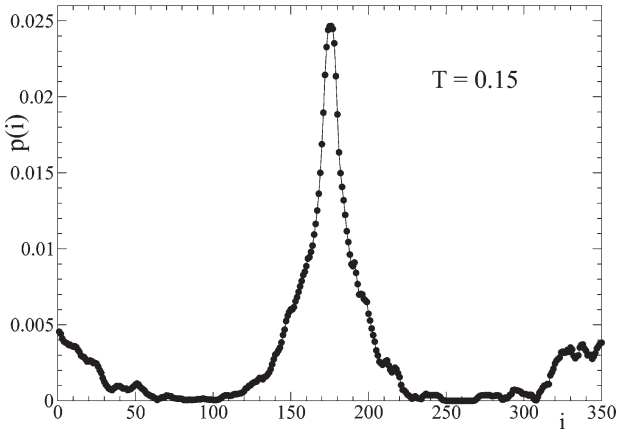

Figure 3. Distribution of interfacial monomers (see text for definition) at $T = 0.15$.

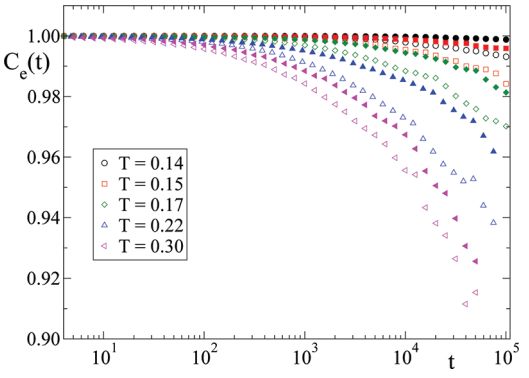

Figure 4. End-to-end correlator at the investigated temperatures. Empty and filled symbols correspond to F- and S-blocks, respectively.

in previous investigations on strongly segregated lamellar phases,[33,34] the local density profiles exhibit, within statistics, a flat structure from the immediate neighborhood of the interface to the center of the domains (see Figure 2b). This is similar to the observation in free-standing films.[51,53,66,67] It is instead rather different from the layering behavior observed near rigid smooth walls, for both free[48,49,53,67] and grafted chains.[68,69] There, the local density profiles exhibit strong oscillations along the z-direction, of increasing amplitude on approaching the wall. As in free-standing films, the mobile and irregular character of the interface seems to frustrate layering in the lamellar domains, leading to the observed flat profiles in Figure 2.

With the used normalization for $\rho(z)$ (see above), we can directly estimate differences between the local density within the domains and the macroscopic density ρ_{hom} of the respective homopolymers. This comparison is shown in detail in Figure 2b. We define the z-position of the interface, z_{int}, as the crossing point of the density profiles $\rho(z)$ of the respective F- and S-domains. We only observe clear differences between $\rho(z)$ and ρ_{hom} in the immediate neighborhood of the interface, at distances $\Delta z = |z - z_{int}| \lesssim 3\sigma$. By mapping to real units (see section II), the latter corresponds to an interfacial half-width of about 1.5−3 nm, in qualitative agreement with experimental values in strongly segregated phases.[20,30,38] In the rest of the domain we find that, within statistics, $\rho(z) = \rho_{hom}$. Therefore, Figure 2 clearly demonstrates that gradients of density (defined as variations of $\rho(z)$ along the domains) are absent and that the density of each homopolymer is unperturbed in the lamellar phase of the diblock system.

Now we identify the type of monomers located near the interfaces. We label the monomers along the chain as $i = 1, 2, ..., N$, from one chain end to the other one, and starting from the F-end. By defining the interface positions z_{int} as above, we can obtain the distribution $p(i)$ of interfacial monomers. For this we compute the histogram of i-monomers which are at a distance $\Delta z < 2\sigma$ from the nearest interface. Results are presented in Figure 3. Not surprisingly, $p(i)$ displays a sharp maximum around $N/2 = 175$. This just reflects the fact that monomers close to the F−S bond (in the following denoted as *junction monomers*) are preferentially located in the immediate neighborhood of the interface. There are other types of monomers which also follow the criterium $\Delta z < 2\sigma$. Such monomers are those close to the block ends[34,70] (in the following denoted as *end monomers*), as indicated (see Figure 3) by the two secondary peaks of $p(i)$ in the ranges $i \lesssim 50$ and $i \gtrsim 300$. The presence of these secondary peaks is easily understood by inspection of the bottom panel of Figure 1, which shows that stretched blocks extend from one interface to the next one. The contribution of end monomers to the total population of interfacial monomers is significant. Indeed, we estimate such a contribution, by simple integration of $p(i)$, as about a 25% of the total. Having noted the significant fraction of end monomers at the interface, these can be also found at any region of the domains. This is demonstrated by representing the corresponding density profiles $\rho(z)$ of end monomers (see Figure 2a).

Still, the results presented in Figures 2 and 3 for the distribution of end monomers should be taken with care. It must be noted that full equilibration at large scales is extremely difficult for the long investigated chains, even by preparing the system in the lamellar geometry. This is evidenced by representing the end-to-end orientational correlator $C_e(t) = \langle \mathbf{R}(t)\cdot\mathbf{R}(0)\rangle/\langle R^2(0)\rangle$, with $\mathbf{R}$ the vector joining the junction and end monomer of each block. Figure 4 shows results of $C_e(t)$ for both F- and S-blocks at the investigated temperatures. Not surprisingly for the simulated long chains, $C_e(t)$ shows very weak relaxation; i.e., block reorientations are far from being completed in the time scale of the simulation. Thus, large scale equilibration cannot be guaranteed even by using the box length search algorithm (see above). Full reorientations within the simulation window could only be achieved by simulating much shorter nonentangled chains, which however would lead to domain sizes much smaller than the experimentally relevant values investigated here. Having noted this, we believe that, because of the achieved balance of the three components of the pressure (see above), the obtained structures should be reasonably close to the real equilibrium ones. Thus, minor differences between the obtained chain conformations and the equilibrium ones would have no significant effects on the qualitative trends observed at local scales for the segmental α-relaxation.

B. Dynamics. Now we discuss dynamic features in the lamellar phase. Panel a of Figure 5 displays results for the T-dependence of the mean-squared displacement, $\langle \Delta r^2(t)\rangle$, of F- and S-monomers in the diblock system. The corresponding results for the orientational correlator, $P(t)$, of F−F and S−S bonds are shown in panel b. The bond orientational correlator is defined as $P(t) = \langle \cos\theta(t)\rangle$, with $\theta(t)$ the angle between the orientations of the bond at $t = 0$ and at the considered t. As usual in two-component polymer systems,[71] a progressive dynamic separation

dx.doi.org/10.1021/ma200470a |*Macromolecules* 2011, 44, 6952–6961

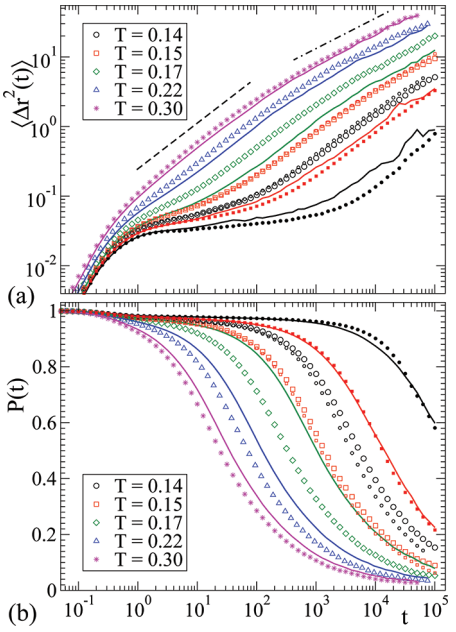

Figure 5. Temperature dependence of the mean-squared displacement of the α-monomers (a) and the orientational correlator of the α−α bonds (b). Large empty symbols and solid lines correspond respectively to α = F and S in the diblock system. Temperatures for solid lines are, from top to bottom, the same as for large empty symbols (see legend). We also include, as small circles ($T = 0.14$) and small squares ($T = 0.15$), the corresponding data for the homopolymers (empty small symbols: F-homopolymer; filled small symbols: S-homopolymer). Dashed and dashed-dotted lines in (a) are power laws $\sim t^{0.65}$ and $\sim t^{0.45}$, respectively.

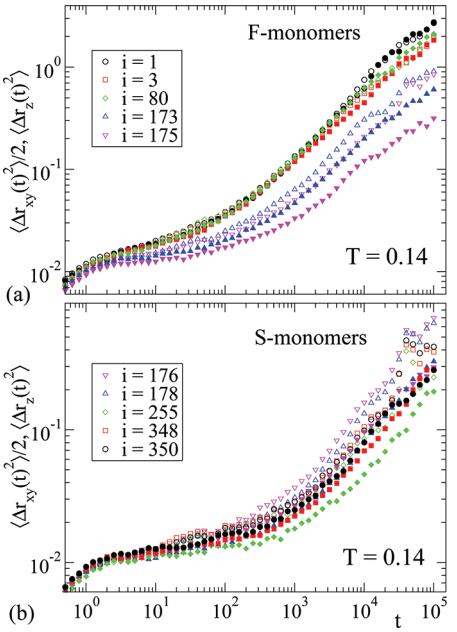

Figure 6. For the diblock system at $T = 0.14$, components of the mean-squared displacement of selected monomers (of index i, see legend). Empty and filled symbols (of identical color for a same i) correspond respectively to $\langle \Delta r_{xy}^2(t)\rangle/2$ and $\langle \Delta r_z^2(t)\rangle$. (a) F-monomers; (b) S-monomers.

between the F- and S-components is observed as temperature decreases. Estimating structural relaxation times τ as those for which $\langle \Delta r^2(\tau)\rangle = \sigma^2$ or $P(\tau) = e^{-1}$, we observe a separation of about 1 decade in τ at the lowest investigated $T = 0.14$ (see Figure 5). For comparison, we have included the corresponding data for the F- and S-homopolymers at the two lowest investigated temperatures $T = 0.14$ and $T = 0.15$. Small differences are observed between the blocks and their respective homopolymers (also for the data at the other temperatures, not shown for the homopolymers). The coupling to a block of lower or higher intrinsic mobility has a different effect on the F- and S-components. Thus, the segmental relaxation in the F-blocks is slightly slower than in the F-homopolymer, in agreement with the usual experimental observation in blocks coupled to a slower component.[30,36,38,40,41,43] In the case of the S-blocks the opposite effect is observed for the mean-squared displacement, which is slightly sped up in comparison with that of the S-homopolymer. However, no clear differences are observed between the orientational correlators of the S-blocks and the S-homopolymer.

After the initial ballistic regime a plateau arises in both $\langle \Delta r^2(t)\rangle$ and $P(t)$, at $t \approx 1$, for $T < 0.22$. The plateau extends over longer time scales as temperature decreases. This feature is a well-known manifestation of the caging regime, i.e., the temporary trapping of each particle by the surrounding ones, which is characteristic of glass-forming liquids on approaching the glass transition temperature.[44,45] The plateau regime (or the ballistic one at high T) is not followed by a crossover to an ultimate diffusive regime $\langle \Delta r^2(t)\rangle \sim t$. It is well-known that prior to it homopolymers exhibit subdiffusive behavior over several time decades, corresponding to Rouse-like dynamics of the internal chain degrees of freedom.[72] Even further subdiffusive regimes, usually assigned to reptation dynamics,[72] arise in the case of long chains as those simulated here, of length $N = 350$ beyond the entanglement value ($N_e \sim 60$ for bead−spring models[73]). How the former pictures for chain dyamics are affected in the lamellar phase, and in particular the effect of the coupling of each block to other with very different mobility, are questions which are beyond the scope of this article and will be discussed elsewhere.

As mentioned in the Introduction, the segmental relaxation of each component may be expected to exhibit dynamic heterogeneity in the lamellar phase. Having noted this, the latter may be moderate at the investigated temperatures. Thus, the mobility of the junction monomers may be enhanced by the surrounding end monomers, which are intrinsically faster and coexist with the former ones near the interface (see Figure 3). This effect may reduce significantly dynamic differences between junction and end monomers. In order to elucidate this point, we show in Figure 6, at fixed $T = 0.14$, the mean-squared displacements of some selected monomers. These results provide a comparison between the dynamics of end monomers ($i = 1$, 3, 348, and 350) and junction monomers ($i = 173$, 175, 176, and 178). We also include results for $i = 80$ and 255, corresponding to monomers located at the center of the blocks (in the following denoted as *central monomers*). Moreover, in order to characterize the anisotropy of the monomer motions, we show the components of the displacements parallel, $\langle \Delta r_{xy}^2(t)\rangle = \langle \Delta r_x^2(t) + \Delta r_y^2(t)\rangle$, and perpendicular, $\langle \Delta r_z^2(t)\rangle$, to the lamellar planes. For a correct comparison between both components, data for the parallel component have been rescaled by 1/2. We have selected a reduced set of i-values for clarity of presentation of Figure 6. Having noted this, the former are representative and cover all the spread observed in the distribution of relaxation times. In particular, the different sets of data in the range $10 \lesssim i \lesssim 160$ for the F-monomers and $210 \lesssim i \lesssim 320$ for the S-monomers are

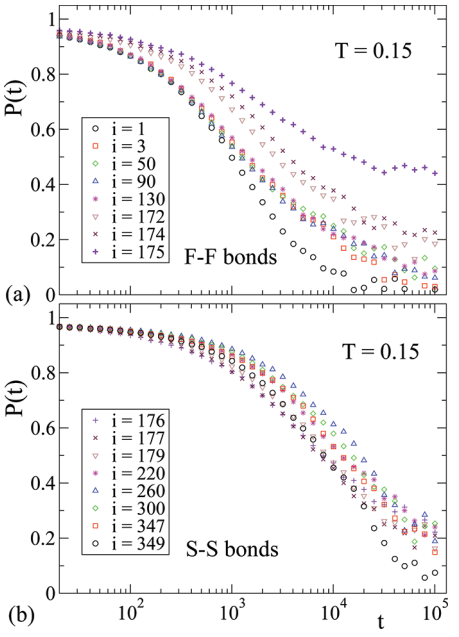

Figure 7. For the diblock system at $T = 0.15$, orientational correlators for selected monomers (of index i, see legend). Results for F−F and S−S bonds are respectively displayed in (a) and (b). Panel (a) also includes the data for the F−S bond ($i = 175$).

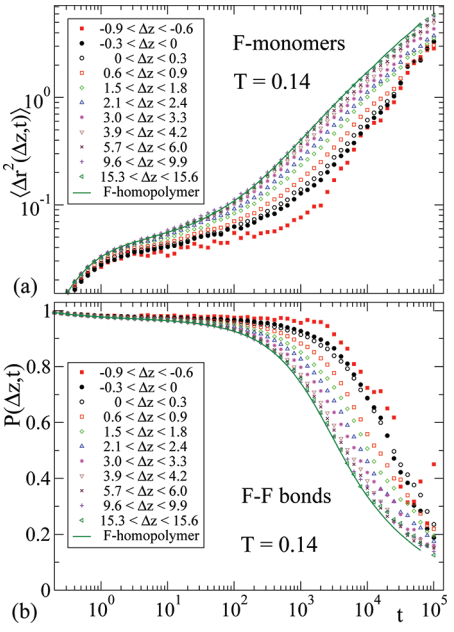

Figure 8. (a) Symbols are mean-squared displacements of F-monomers for different layers (see text). Positive and negative values of Δz correspond to monomers located at $t = 0$ respectively in the F- and S-domains. All data correspond to $T = 0.14$. (b) Same as (a) for the layer-dependent orientational correlators $P(\Delta z,t)$ of the F−F bonds (symbols). Lines in both panels are the data for the F-homopolymer.

hardly distinguishable from respectively the sets $i = 80$ and 255 represented in Figure 6. In other words, we only observe a significant dynamic spread for the interfacial monomers, i.e., for the junction and end monomers.

Dynamic heterogeneity as a function of the location along the chain exhibits different trends for the F- and S-components. For the F-blocks, the junction monomers are slower than the central and end monomers (Figure 6a). This effect is especially visible for the F-monomer directly linked to the S-block ($i = 175$) and in particular for the perpendicular component of the motion, which is strongly slowed down in comparison with the parallel one. No significant anisotropy of the motions is observed for the central and end F-monomers within the length scale for the displacements explored in the simulation time window.[74]

The former dynamic features for the junction F-monomers can be attributed to their coupling to the dynamics of the neighboring S-monomers, which exhibit an intrinsically slower relaxation. Translational motions of the S-monomers show different trends (Figure 6b). In this case the central S-monomers exhibit slower dynamics than the end and junction S-monomers which, according to the distribution $p(i)$ of Figure 3, are close (and then dynamically coupled) to faster monomers of the F-domain. It is not clear whether the observed anisotropy in the decaging regime of the central S-monomers (see set $i = 255$ for $t \gtrsim 10^2$ in Figure 6b) is an statistical artifact. It emerges only at the two lowest investigated temperatures, for which the α-relaxation of the central S-monomers is not fully completed within the simulation window, i.e., $\langle \Delta r^2(t) \rangle < \sigma^2$. Central F-monomers do not show anisotropic motions but note that in this case $\langle \Delta r^2(t) \rangle > \sigma^2$ for all the investigated temperatures. Thus, it might be that the anisotropic motion of central monomers in the uncompleted α-relaxation is a precursor of the anisotropy of vibrations in the glassy state. The stretching and freezing of the chains in the glassy lamellar structure might favor vibrations of slightly larger amplitude in the lateral direction than in the perpendicular one.

In analogy with the former discussion, Figure 7 shows results for the orientational correlators $P(t)$ of selected bonds, at fixed $T = 0.15$. The bond i is defined as that connecting the monomers i and $i + 1$. Thus, $i = 175$ denotes the bond connecting the F- and S-blocks. Reorientation of the junction, end, and central bonds follows similar trends to those exhibited by the monomer translations of both F- and S-species. Not surprisingly, the F−S bond connecting the two blocks exhibits a much slower relaxation than the rest of the bonds. Thus, the reorientation of the F−S bond is strongly hindered by the large activation energy produced by the contact between the different species.

The results of Figures 6 and 7 reveal, for the investigated T-range, a moderate heterogeneity in the segmental dynamics as a function of the location along the chain. Similar results are obtained as a function of the distance to the nearest interface. We introduce the layer-dependent mean-squared displacement $\langle \Delta r^2(z_{min} < \Delta z < z_{max}, t) \rangle$, defined as the average over the α-monomers ($\alpha \in \{F,S\}$) which are initially (i.e., at $t = 0$) located in a layer at a z-distance $z_{min} < \Delta z < z_{max}$ from the nearest interface. Each data set for α-monomers ($\alpha \in \{S,F\}$) is averaged over two layers, both at a distance Δz of one of the two interfaces delimiting the corresponding α-domain. Obviously $0 \leq |\Delta z| \leq d/2$, with d the domain size. Positive or negative values of Δz correspond to monomers initially located in domains of respectively their same or the other species. Likewise, we introduce the orientational correlator $P(z_{min} < \Delta z < z_{max}, t)$ for α−α bonds. We consider that a bond is initially located at a given layer if its center-of-mass fulfills at $t = 0$ the condition $z_{min} < \Delta z < z_{max}$. By introducing the former observables for layers perpendicular to the lamellar planes, we characterize the dynamic heterogeneity as a function of the distance to the nearest interface.

dx.doi.org/10.1021/ma200470a |*Macromolecules* 2011, 44, 6952–6961

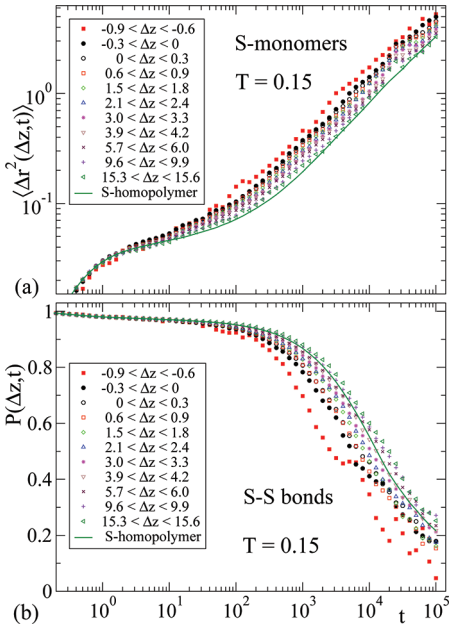

Figure 9. As in Figure 8 for S-monomers and S−S bonds. All data correspond to $T = 0.15$.

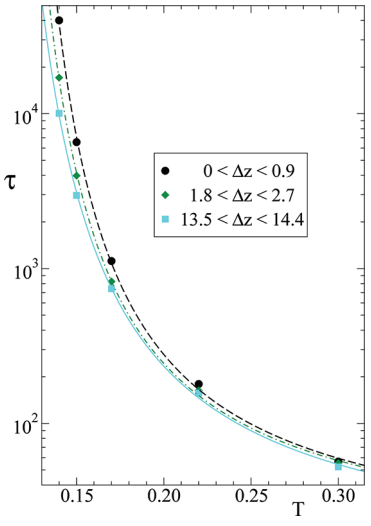

Figure 10. Symbols: relaxation times of the correlators $P(\Delta z,t)$ for the F−F bonds in three selected layers. Lines: fits to an VFT law $\tau = \tau_\infty \exp[E/k_B(T - T_0)]$.

Figure 8 shows results, at $T = 0.14$, of $\langle \Delta r^2(\Delta z,t)\rangle$ for the F-monomers (a) and of $P(\Delta z,t)$ for the F−F bonds (b). A moderate dispersion, over about 1 decade, is again observed in the respective relaxation times. Not surprisingly, the relaxation of the F-monomers and F−F bonds initially located at layers within the slow S-domain is slower than the relaxation of those located at the center of the F-domains, with a monotonic crossover between both limits. The dynamics of the F-homopolymer is recovered as the center of the F-domain is approached. Thus, for distances $\Delta z \gtrsim 4\sigma$ from the nearest interface the data for the F-blocks are almost indistinguishable from those of the F-homopolymer. Figure 9 shows, for $T = 0.15$,[75] the corresponding results of $\langle \Delta r^2(\Delta z,t)\rangle$ and $P(\Delta z,t)$ for the S-monomers and S−S bonds. In this case the structural relaxation is slowed down and approaches that of the S-homopolymer on moving from the interface to the center of the S-domain.

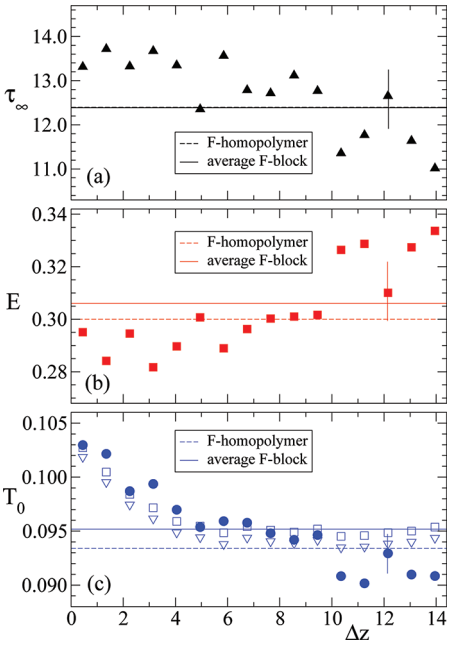

Figure 11. Horizontal lines: VFT parameters for the relaxation times of the global correlators $P(t)$ for the F-blocks (solid lines) and the F-homopolymer (dashed lines). Symbols: VFT parameters for the relaxation times of the layer-dependent correlators $P(\Delta z,t)$ for the F−F bonds. Data in (a), (b), and (c) correspond respectively to τ_∞, E, and T_0. Filled symbols are data obtained from fully free fits. Vertical lines are typical error bars. Empty symbols in (c) are data obtained from VFT fits with free T_0 and fixed values of τ_∞ and E. Namely, we fix $\tau_\infty = 12.4$, i.e, the value obtained for the global $P(t)$ of both the F-homopolymer and the F-blocks [see panel (a)]. For the VFT activation energy we fix $E = 0.300$ (squares) and $E = 0.306$ (triangles), which are respectively the values obtained for the global $P(t)$ in the F-homopolymer and in the F-blocks [see horizontal lines in panel (b)].

IV. DISCUSSION

As for the global bond correlators $P(t)$, we define the relaxation times τ for the layer-dependent correlators as the times at which $P(\Delta z,\tau) = e^{-1}$. We have fitted the so-obtained relaxation times for the F−F bonds to an empirical Vogel−Fulcher−Tamann (VFT) law, $\tau = \tau_\infty \exp[E/k_B(T - T_0)]$. The latter is usually invoked in the analysis of the structural relaxation in glass-forming systems.[44,45] Figure 10 shows some representative fits for F−F bonds close to the interface and at the center of the F-domains. The fit parameters τ_∞, E, and T_0 are displayed in Figure 11 as a function of the layer position.[76] For comparison, we include the results for the global correlator $P(t)$ (i.e, averaged over all the F−F bonds), both for the F-blocks in the lamellar phase and for the F-homopolymer.

The values of the VFT parameters for $P(\Delta z,t)$, obtained from the fully free fits, vary with the distance to the interface. The VFT parameters are strongly coupled, and descriptions with the same quality of Figure 10 can be achieved by means of slight variations of those obtained from the fully free fits (see error bars in Figure 11). This is the case by leaving T_0 as the only free parameter and fixing the values of the attemp period τ_∞ and

dx.doi.org/10.1021/ma200470a |Macromolecules 2011, 44, 6952–6961

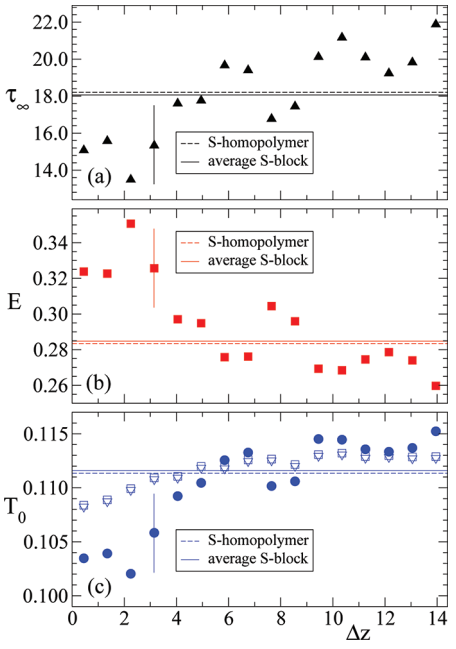

Figure 12. As in Figure 11 for the S-component.

the VFT activation energy E. Namely we fix $\tau_\infty = 12.4$, i.e., the value obtained for the global $P(t)$ of both the F-homopolymer and the F-blocks in the lamellar phase (Figure 11a). For the VFT activation energy we select two fixed values $E = 0.300$ and $E = 0.306$. These very similar values are those obtained for the global $P(t)$ of respectively the F-homopolymer and the F-blocks in the lamellar phase (Figure 11b). Not surprisingly, this fitting scheme with fixed τ_∞ and E yields a smoother layer-dependence of T_0 than in the fully free fit (see Figure 11c). The so-obtained $T_0(\Delta z)$ decreases by moving from the interface to the center of the F-domain. Initially, it shows a sharp decay, until a distance from the interface of about 4σ, for which the T_0 of the F-homopolymer is already approached. This is consistent with the relaxation of $P(\Delta z,t)$ observed in Figure 8b, which is similar to that of the F-homopolymer for $\Delta z \gtrsim 4\sigma$, while it is slowed down on approaching the interface (as expected from an increasing T_0).

Figure 12 shows the corresponding VFT parameters for the correlators of the S−S bonds. The parameters obtained from fully free fits show opposite trends to those of Figure 11 for the F−F bonds. It is noteworthy that the interfacial effects for $T_0(\Delta z)$ seem to emerge again in the range $\Delta z \lesssim 4\sigma$. A forced fit by fixing the values of τ_∞ and E to those of the S-homopolymer seems less justified than in the case of the F−F bonds. Indeed the so-obtained values of $T_0(\Delta z)$ exhibit, near the interface, a much weaker variation than those obtained from fully free fits. Having said this, it must be noted that, unlike for the F−F bonds, at $T = 0.14$ the orientational correlators for the S−S bonds do not decay to e^{-1} within the simulation window, and therefore the corresponding relaxation times τ at $T = 0.14$ are not available for the corresponding VFT fits. For this reason the VFT parameters from fully free fits in Figure 12 have larger uncertainties than those for the F−F bonds in Figure 11, and the discrepancies between the different sets of $T_0(\Delta z)$ in Figure 12c must be taken with care.

In the following we discuss the results obtained for the fast F-component in comparison with experimental observations. In particular, we construct layer-dependent VFT curves according

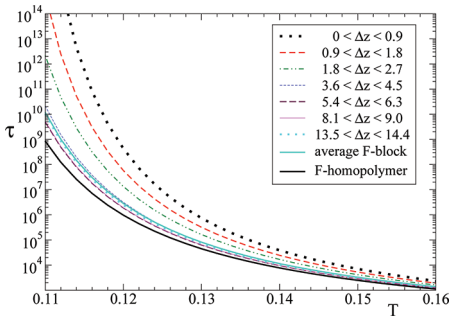

Figure 13. VFT curves for the reorientation of the F−F bonds, extrapolated to low temperatures (see text for details).

to the analysis performed by Lorthioir et al. in ref 38 for BDS data of the structural relaxation of poly(dimethylsiloxane) (PDMS) in the diblock lamellar phase with poly(styrene) (PS). It must be noted that PDMS ($T_g \approx 145$ K) has a lower glass transition temperature than PS ($T_g \approx 370$ K), and therefore the F-homopolymer in the present model qualitatively plays the role of the PDMS. By taking the values of $T_0(\Delta z)$ for fixed $\tau_\infty = 12.4$ and $E = 0.300$ (empty squares in Figure 11c), we construct for each layer the corresponding VFT curve extrapolated to low temperatures, below the range investigated by simulations. Indeed, the analysis of ref 38 is equivalent to assume, as in our case, values of τ_∞ and E constant and identical to those of the corresponding homopolymer and leaving $T_0(\Delta z)$ as the only layer-dependent parameter.

The extrapolated VFT curves for the reorientation of the F−F bonds are shown in Figure 13. The set of curves (not shown) constructed with the VFT parameters obtained from fully free fits (filled symbols in Figure 11) exhibit the same qualitative trends. The relaxation times for the different layers progressively spread as temperature decreases. Thus, by assuming the validity of the extrapolation, we observe at $T = 0.113$ a variation in the relaxation times of about 5 decades from the interface to the center of the F-domains. At the former temperature the relaxation time in the immediate neighborhood of the interface is 10^{14}, which roughly corresponds to 10^2-10^3 s in real systems (see section II), i.e., the usual time scale for defining the laboratory glass transition temperature.[44,45] Consistently with the observations in Figures 8b and 11c, the observed spread in the relaxation times esentially emerges at distances from the interface smaller than about 4σ. Note that the small differences in the extrapolated VFT curves at large values of Δz originate from the statistical error in the used values of $T_0(\Delta z)$ (see Figure 11c).

The results of Figures 8, 11, and 13 are consistent with the physical interpretation of the experiments of ref 38, which proposes the existence of gradients of mobility originating from gradients of VFT temperatures, $T_0(\Delta z)$. The dynamic range probed by the global response of the PDMS segments in ref 38 extends over frequencies lower than 10^5 Hz. By using the conversion factors from simulation to real units (see section II), the former dynamic range qualitatively correspons to temperatures for which the relaxation time of the global $P(t)$ is $\tau \gtrsim 10^7$. At such temperatures the layer-dependent times of Figure 13 spread over at least 3 decades. This is qualitatively consistent with the distributions of times $\tau(\Delta z)$ obtained from the experimental analysis of ref 38. There it is also proposed that the gradients of mobility extend from the interface to some distance d, beyond which the PDMS segments in the lamellar domains

esentially follow the same dynamic behavior as in the PDMS homopolymer. The estimated spatial extension of the gradients is $d \sim 4$ nm.[38] This value is qualitatively consistent with the distance, $\Delta z \approx 4\sigma$, at which the VFT temperature $T_0(\Delta z)$ and layer-dependent dynamic observables approach those of the F-homopolymer in our simulations (see Figures 8, 11, and 13).

According to the interpretation of ref 38, the gradients of mobility, which are directly related with the obtained gradients of VFT temperatures $T_0(\Delta z)$, originate from gradients of density. Inspection of Figures 2 and 11 suggests that the latter is esentially an interfacial effect. Thus, $\rho(\Delta z)$ and $T_0(\Delta z)$ become constant (layer-independent) and equal within error bars to the values for the F-homopolymer, at similar distances from the interface. These distances are $\Delta z \gtrsim 3\sigma$ for $\rho(\Delta z)$ (Figure 2) and $\Delta z \gtrsim 4\sigma$ for $T_0(\Delta z)$ (Figure 11).

V. CONCLUSIONS

We have performed simulations of a simple bead−spring model for strongly segregated lamellar phases of diblock copolymers, with blocks of different mobility. We have characterized the heterogeneity of the segmental dynamics associated with the glass transition. This has been done by computing monomer translations and bond reorientations as a function of both the location along the chain and the distance to the nearest interface. This analysis reveals moderate gradients of mobility in the investigated temperature range, which qualitatively probes time scales of up to hundreds of nanoseconds. Thus, the obtained distribution of relaxation times spreads over about 1 decade. This result is relevant for the interpretation of experiments probing the former dynamic window, e.g., by means of neutron spin-echo techniques,[77] suggesting that strong gradients of mobility and broad distributions of relaxation times should not be invoked in the data analysis.

However, the extrapolation of the simulation results to lower temperatures (i.e., to much longer time scales) suggests an increasing dispersion over several time decades. The extrapolated results are consistent with the interpretation of BDS experiments, which relate gradients of mobility with gradients of the VFT temperature. The simulations reveal, for the fast block, a decrease of the VFT temperature on moving from the interface to the center of the lamellar domain. The opposite effect is observed for the slow block. The structural relaxation and VFT temperature within the lamellar domains approach those of the respective homopolymers at a distance from the interface of about 2−4 nm, in agreement with proposed values from BDS experiments. This distance roughly corresponds to the interfacial thickness. Therefore, gradients of mobility emerge esentially as an interfacial effect. They are not related with long-range gradients of density along the lamellar domains. The latter are indeed absent, and the density of the corresponding homopolymers is only perturbed in the interfacial region.

AUTHOR INFORMATION

Corresponding Author

*E-mail: wabmosea@ehu.es.

ACKNOWLEDGMENT

We thank A. Alegría for useful discussions. We acknowledge financial support from the projects MAT2007-63681 (Spain), IT-436-07 (GV, Spain), and FP7-PEOPLE-2007-1-1-ITN (DYNACOP, EU).

REFERENCES

(1) Bates, F. S.; Fredrickson, G. H. *Annu. Rev. Phys. Chem.* **1990**, *41*, 525.
(2) Fredrickson, G. H.; Bates, F. S. *Annu. Rev. Mater. Sci.* **1996**, *26*, 501.
(3) Alexandridis, P., Lindman, B., Eds.; *Amphiphilic Block Copolymers*; Elsevier: Amsterdam, Netherlands, 2000.
(4) Matsen, M. W.; Bates, F. S. *Macromolecules* **1996**, *29*, 1091.
(5) Matsen, M. W. *J. Phys.: Condens. Matter* **2002**, *14*, R21.
(6) Hajduk, D. A.; Harper, P. E.; Gruner, S. M.; Honeker, C. C.; Kim, G.; Thomas, E. L.; Fetters, L. J. *Macromolecules* **1994**, *27*, 4063.
(7) Ko, M. B.; Mattice, W. L. *Macromolecules* **1995**, *28*, 6871.
(8) Hamersky, M. W.; Hillmyer, M. A.; Tirrell, M.; Bates, F. S.; Lodge, T. P.; von Meerwall, E. D. *Macromolecules* **1998**, *31*, 5363.
(9) Cavicchi, K. A.; Lodge, T. P. *Macromolecules* **2004**, *37*, 6004.
(10) Khanna, V.; Kim, B. J.; Hexemer, A.; Mates, T. E.; Kramer, E. J.; Li, X.; Wang, J.; Hahn, S. F. *Macromolecules* **2007**, *40*, 2443.
(11) Willner, L.; Lund, R.; Monkenbusch, M.; Holderer, O.; Colmenero, J.; Richter, D. *Soft Matter* **2010**, *6*, 1559.
(12) Rittig, F.; Kärger, J.; Papadakis, C. M.; Fleischer, G.; Almdal, K.; Štěpánek, P. *Macromolecules* **2001**, *34*, 868.
(13) Hoffmann, A.; Sommer, J. U.; Blumen, A. *J. Chem. Phys.* **1997**, *107*, 7559.
(14) Yokoyama, H.; Kramer, E. J. *Macromolecules* **1998**, *31*, 7871.
(15) Fleischer, G.; Rittig, F.; Kärger, J.; Papadakis, C. M.; Mortensen, K.; Almdal, K.; Štěpánek, P. *J. Chem. Phys.* **1999**, *111*, 2789.
(16) Yokoyama, H.; Kramer, E. J.; Fredrickson, G. H. *Macromolecules* **2000**, *33*, 2249.
(17) Cavicchi, K. A.; Lodge, T. P. *Macromolecules* **2003**, *36*, 7158.
(18) Papadakis, C. M.; Rittig, F.; Almdal, K.; Mortensen, K.; Štěpánek, P. *Eur. Phys. J. E* **2004**, *15*, 359.
(19) Moreno, A. J.; Colmenero, J. *Macromolecules* **2009**, *42*, 8543.
(20) Lund, R.; Willner, L.; Alegría, A.; Colmenero, J.; Richter, D. *Macromolecules* **2008**, *41*, 511.
(21) Stühn, B.; Stickel, F. *Macromolecules* **1992**, *25*, 5306.
(22) Ehlich, D.; Takenaka, M.; Hashimoto, T. *Macromolecules* **1993**, *26*, 492.
(23) Dalvi, M. C.; Eastman, C. E.; Lodge, T. P. *Phys. Rev. Lett.* **1993**, *71*, 2591.
(24) Dalvi, M. C.; Lodge, T. P. *Macromolecules* **1993**, *26*, 859.
(25) Hoffmann, A.; Koch, T.; Stühn, B. *Macromolecules* **1993**, *26*, 7288.
(26) Haliloglu, T.; Balaji, R.; Mattice, W. L. *Macromolecules* **1994**, *27*, 1473.
(27) Lodge, T. P.; Dalvi, M. C. *Phys. Rev. Lett.* **1995**, *75*, 657.
(28) Karatasos, K.; Anastasiadis, S. H.; Floudas, G.; Fytas, G.; Pispas, S.; Hadjichristidis, N.; Pakula, T. *Macromolecules* **1996**, *29*, 1326.
(29) Hoffmann, A.; Sommer, J. U.; Blumen, A. *J. Chem. Phys.* **1997**, *106*, 6709.
(30) Alig, I.; Floudas, G.; Avgeropoulos, A.; Hadjichristidis, N. *Macromolecules* **1997**, *30*, 5004.
(31) Pakula, T.; Karatasos, K.; Anastasiadis, S. H.; Fytas, G. *Macromolecules* **1997**, *30*, 8463.
(32) Hamersky, M. W.; Tirrell, M.; Lodge, T. P. *Langmuir* **1998**, *14*, 6974.
(33) Murat, M.; Grest, G. S.; Kremer, K. *Europhys. Lett.* **1998**, *42*, 401.
(34) Murat, M.; Grest, G. S.; Kremer, K. *Macromolecules* **1999**, *32*, 595.
(35) Anastasiadis, S. H.; Rittig, F.; Chrissopoulou, K.; Fleischer, G.; Fytas, G.; Semenov, A. N.; Kärger, J.; Xenidou, M.; Pispas, S.; Hadjichristidis, N. *Europhys. Lett.* **2000**, *51*, 68.
(36) Kyritsis, A.; Pissis, P.; Mai, S.-M.; Booth, C. *Macromolecules* **2000**, *33*, 4581.

(37) Dollase, T.; Graf, R.; Heuer, A.; Spiess, H. W. *Macromolecules* **2001**, *34*, 298.
(38) Lorthioir, C.; Alegría, A.; Colmenero, J.; Deloche, B. *Macromolecules* **2004**, *37*, 7808.
(39) Müller, M.; Daoulas, K. C. *J. Chem. Phys.* **2009**, *129*, 164906.
(40) Encinar, M.; Guzmán, E.; Prolongo, M. G.; Rubio, R. G.; Sandoval, C.; González-Nilo, F.; Gargallo, L.; Radić, D. *Polymer* **2008**, *49*, 5650.
(41) Mok, M. M.; Masser, K. A.; Runt, J.; Torkelson, J. M. *Macromolecules* **2010**, *43*, 5740.
(42) del Valle-Carrandi, L.; Alegría, A.; Colmenero, J. *Eur. Phys. J.: Spec. Top.* **2010**, *189*, 257.
(43) Sanz, A.; Nogales, A.; Ezquerra, T. A. *Soft Matter* **2011**, *7*, 6477.
(44) Debenedetti, P. G. *Metastable Liquids*; Princeton University Press: Princeton, 1996.
(45) Binder, K.; Kob, W. *Glassy Materials and Disordered Solids*; World Scientific: Singapore, 2005.
(46) Lai, P.-Y.; Binder, K. *J. Chem. Phys.* **1992**, *97*, 586.
(47) Neelov, I. M.; Binder, K. *Macromol. Theory Simul.* **1995**, *4*, 1063.
(48) Baschnagel, J.; Varnik, F. *J. Phys.: Condens. Matter* **2005**, *17*, R851.
(49) Varnik, F.; Baschnagel, J.; Binder, K. *Phys. Rev. E* **2002**, *65*, 021507.
(50) Torres, J. A.; Nealey, P. F.; de Pablo, J. J. *Phys. Rev. Lett.* **2000**, *85*, 3221.
(51) Morita, H.; Tanaka, K.; Kajiyama, T.; Nishi, T.; Doi, M. *Macromolecules* **2006**, *39*, 6233.
(52) Peter, S.; Napolitano, S.; Meyer, H.; Wübbenhorst, M.; Baschnagel, J. *Macromolecules* **2008**, *41*, 7729.
(53) Peter, S.; Meyer, H.; Baschnagel, J. *J. Polym. Sci., Part B: Polym. Phys.* **2006**, *44*, 2951.
(54) Scheidler, P.; Kob, W.; Binder, K. *Europhys. Lett.* **2000**, *52*, 277.
(55) Scheidler, P.; Kob, W.; Binder, K. *J. Phys. Chem. B* **2004**, *108*, 6673.
(56) Eral, H. B.; van den Ende, D.; Mugele, F.; Duits, M. H. G. *Phys. Rev. E* **2009**, *80*, 061403.
(57) Kremer, K.; Grest, G. S. *J. Chem. Phys.* **1990**, *92*, 5057.
(58) Frenkel, D.; Smit, B. *Understanding Molecular Simulation*; Academic Press: San Diego, 1996.
(59) The total energy of the system is not strictly conserved. Numerical integration of the equations of motion leads to a weak but systematic drift of the latter with respect to the initial value, E_0, at the beginning of the production run. Whenever the relative drift $|1 - E(t)/E_0|$ at a given time t is larger than 10^{-3}, the kinetic energy is corrected by means of velocity scaling, in order to recover the inital value E_0. This correction is irrelevant within the fluctuations of T and is performed a few times during the production run, which is also irrelevant for the dynamics. Thus, the typical time (in simulation units) between consecutive corrections is $\sim 10^4$. With these irrelevant corrections, ensemble average is essentially microcanonical.
(60) Martyna, G. J.; Tuckerman, M. E.; Tobias, D. J.; Klein, M. L. *Mol. Phys.* **1996**, *87*, 1117.
(61) Anderson, J. A.; Lorenz, C. D.; Travesset, A. *J. Chem. Phys.* **2008**, *128*, 184906.
(62) Grest, G. S.; Lacasse, M. D.; Kremer, K.; Gupta, A. M. *J. Chem. Phys.* **1996**, *105*, 10583.
(63) Loison, C.; Mareschal, M.; Kremer, K.; Schmid, F. *J. Chem. Phys.* **2003**, *119*, 13138.
(64) Schultz, A. J.; Hall, C. K.; Genzer, J. *J. Chem. Phys.* **2004**, *120*, 2049.
(65) Almdal, K.; Rosedale, J. H.; Bates, F. S.; Wignall, G. D.; Fredrickson, G. H. *Phys. Rev. Lett.* **1990**, *65*, 1112.
(66) Jain, T. S.; de Pablo, J. J. *Phys. Rev. Lett.* **2004**, *92*, 155505.
(67) Baljon, A. R. C.; van Weert, M. H. M.; de Graaff, R. B.; Khare, R. *Macromolecules* **2005**, *38*, 2391.
(68) Gulati, H. S.; Hall, C. K.; Jones, R. L.; Spontak, R. J. *J. Chem. Phys.* **1996**, *105*, 7712.
(69) Pastorino, C.; Binder, K.; Kreer, T.; Müller, M. *J. Chem. Phys.* **2006**, *124*, 064902.
(70) Yang, J.; Winnik, M. A.; Pakula, T. *Macromol. Theory Simul.* **2005**, *14*, 9.
(71) Arbe, A.; Colmenero, J. *Soft Matter* **2007**, *3*, 1474.
(72) Doi, M.; Edwards, S. F. *The Theory of Polymer Dynamics*; Oxford University Press: Oxford, UK, 1986.
(73) Everaers, R.; Sukumaran, S. K.; Grest, G. S.; Svaneborg, C.; Sivasubramanian, A.; Kremer, K. *Science* **2004**, *303*, 823.
(74) Note that, at least for the perpendicular component, a saturation of the mean-squared displacement is expected in lamellar phases, for long time scales beyond the structural α-relaxation.[26,39] This feature originates from the attachment of the blocks to the lamellar interface, creating extremely large effective barriers for perpendicular diffusion. This saturation persists over much longer time scales, prior to the final crossover to diffusion at times far beyond the simulation window. As observed in experiments,[23,24,27,35] strong entanglement effects for long chains as those investigated here may considerably reduce the anisotropy of the long-time diffusivity.
(75) Unlike in Figure 8 for the F−F bonds, data at $T = 0.14$ for the S−S bonds only exhibit partial relaxation, $P(\Delta z, t_{sim}) > e^{-1}$, at the end of the simulation window t_{sim}. Therefore, we show data for $T = 0.15$ in Figure 9.
(76) Note that Δz is bounded by half the domain size. The latter shrinks with increasing temperature, and only data for $\Delta z \leq 14.4$ are available at all the investigated temperatures. VFT fits are restricted to that range.
(77) Richter, D.; Monkenbusch, M.; Arbe, A.; Colmenero, J. Neutron Spin Echo in Polymer Systems. In *Advances in Polymer Science*; Springer-Verlag: Berlin, 2005; Vol. 174.